Received 19 December 2023; accepted 19 January 2024. Date of publication 10 May 2024; date of current version 4 June 2024.
The review of this paper was arranged by Associate Editor Edoardo Fiorucci.

Digital Object Identifier 10.1109/OJIM.2024.3399250

Robust Band-Pass Filter-Based PLL-Less Approach for Three-Phase Nonsinusoidal Grid Conditions

MANISH KUMAR[1], ANANT KUMAR VERMA[2] (Member, IEEE), CLAUDIO BURGOS-MELLADO[2] (Senior Member, IEEE), RAJ KUMAR JARIAL[1] (Member, IEEE), RAVINDER NATH[1], BHUMAIAH JULA[1], DIEGO MUÑOZ-CARPINTERO[2] (Member, IEEE), CATALINA GONZÁLEZ-CASTAÑO[3], AND PEDRO RONCERO-SÁNCHEZ[4] (Senior Member, IEEE)

[1]Electrical Engineering Department, National Institute of Technology Hamirpur, Hamirpur 177005, India

[2]Electric Power Conversion Systems Laboratory (SCoPE Lab), Universidad de O'Higgins, Rancagua 2841959, Chile

[3]Energy Transformation Center, Engineering Faculty, Universidad Andres Bello, Región Metropolitana, Santiago 7500971, Chile

[4]Department of Electrical, Electronics, Control Engineering and Communications, University of Castilla-La Mancha, 13071 Ciudad Real, Spain

CORRESPONDING AUTHOR: A. K. VERMA (e-mail: anant.kumar@uoh.cl)

This work was supported by the Agencia Nacional de Investigación y Desarrollo (ANID) under Grant ANID/FONDECYT Iniciación/11220989.

ABSTRACT The performance enhancement of an inverter-based grid-connected system necessitates a fast and accurate dynamic response in terms of estimating three-phase grid voltage attributes. The synchronous reference frame phase-locked loop (PLL) and/or the frequency-locking (i.e., frequency-locked loop) approaches are widely used in practical applications. However, due to the phase/frequency feedback loops, the aforementioned parameter estimation schemes may experience instability and provide a slow dynamic response. This work presents a PLL-less grid synchronization solution for three-phase applications to counter the slower dynamic response and demonstrate better immunity against the nonideality of a three-phase grid. In order to remove even and odd-order harmonics and extract the fundamental frequency positive sequence (FFPS), the proposed method employs a combination of band pass filters (CBPFs). Additionally, a novel frequency estimation algorithm is developed, which accurately estimates the angular three-phase grid frequency. Furthermore, the phase angle and amplitude are adaptively estimated using an off-line error-resolving approach, which is derived from the transfer function of the proposed prefiltering solution. Finally, the experimental findings validate the robustness of the current proposal.

INDEX TERMS Amplitude estimation, band pass filter (BPF), frequency estimation, grid synchronization, phase estimation, three-phase system.

NOMENCLATURE

BPF	Band-pass filter.
CBPF	Combined BPF.
DFT	Discrete Fourier transform.
DSC	Delayed signal cancellation.
3ES	Three equidistant samples.
FEA	Frequency estimation algorithm.
FFPS	Fundamental frequency positive sequence.
LPF	Low-pass filter.
NF	Notch filter.
NS	Negative sequence.
PS	Positive sequence.
RE	Relative error.
RESs	Renewable energy sources.
V_{ao}, V_{bo}, V_{co}	Dc-offset present in phase 'a', 'b', and 'c,' respectively.
$\hat{A}_g, A_{\mathrm{m}}$	Estimated instantaneous amplitude of FFPS, Amplitude multiplication factor.
$\hat{A}_{\mathrm{act}}$	Estimated actual value of amplitude of FFPS.
$\hat{f}_g, \Delta\hat{f}_g$	The estimated frequency of the grid voltage, and the deviation of the estimated frequency from the nominal frequency.
f_o, f_s	Nominal frequency, sampling frequency.

h^+, h^-	Harmonic order for PS and harmonic order for NS.
n	Sampling index.
M	Sample length in frequency estimation.
T_o, T_s	Fundamental time period, sampling time period.
v_a, v_b, v_c	Grid voltage in 'abc' frame of phase 'a', 'b', and 'c,' respectively.
v_α, v_β	Input voltage of DFT-BPF.
$\hat{v}^+_{\alpha,1}, \hat{v}^+_{\beta,1}$	Extracted FFPS components extracted by CBPF.
$\vec{v}_{\alpha\beta}$	Output voltage vector of Clarke transform.
$\theta_e, \hat{\theta}_g, \hat{\theta}_{act}$	Phase-angle error correction factor, instantaneous and actual phase angle.

I. INTRODUCTION

THE EMERGING technological trends suggest that the RESs will be crucial in mitigating the detrimental effects of climate change. RES is the primary source for achieving this objective [1]. The healthy operation of a utility grid is ensured when the inverter-based RESs are working in unison, thus, grid synchronization is a crucial prerequisite [2], [3]. Moreover, it is essential to constantly sense the utility voltage signal to predict the state of a healthy grid and keep good command over the grid following inverter [4]. Hence, the measurement systems and the control system of an inverter-based RES are seriously engrossed by the multiple orders of harmonics and interharmonics existing in the utility grid. Nevertheless, the conditioning monitoring stage of an inverter system may also induce deliberate dc-offset, thus, complicating the task of fundamental angular grid frequency, amplitude, and phase angle detection for interfacing RES with the utility grid [5], [6]. Compared to other grid synchronization techniques in the literature, the phase-locked loop (PLL) is the most widely used and recognized method. For estimating grid voltage attributes in three-phase industrial applications, the synchronous reference frame-based PLL (SRF-PLL) is a popular variant [7], [8], [9], [10], [11], [12], [13], [14], [15], [16]. However, under contaminated grid conditions, the SRF-PLL's performance can be unsatisfactory, exhibiting significant oscillations in the estimated grid values in steady state [7], [8]. Although reducing the SRF-PLL bandwidth can alleviate this problem, it comes at the cost of a slow response time, which may not be acceptable, particularly in weak grid conditions where a fast dynamic response is required. Different filtering solutions can be used to improve the SRF-PLL's performance in contaminated grid conditions, but this comes at the expense of slower dynamic response times when compared to other solutions [9].

Generally speaking, the literature on filtering solutions for SRF-PLL typically describes in-loop filtering [10], [11], [12], prefiltering [13], [14], [15], or a combination of both [16]. The in-loop filtering methods include moving average filters (MAFs) [10] which are well-studied owing to their reduced complexity, NFs [11] are another class of filters that can easily counter even-order components in the input signal, proportional-integral-derivative (PID) controllers [12] can act as higher-order LPFs, incorporated particularly for harmonics rejection. However, the inclusion of these filters in the SRF-PLL results in additional phase delay under off-nominal frequencies. Another popular type of filtering method is pre-filtering, intended to reduce the burden on SRF-PLL under distorted grid conditions. Basically, MAFs [13], NFs [14], and DSC [15], are commonly effective in unbalanced and distorted conditions. Second-order generalized integrators (SOGIs) [17], [18] and derivative-based orthogonal signal generators (OSGs) [19] are the most common examples of single-phase OSGs in prefiltering. Using LPFs and OSGs, in-phase and quadrature-phase signals are delivered to the instantaneous symmetrical component (ISC) to extract FFPS from the contaminated three-phase grid voltage. This requires extensive mathematical computations, increasing the complexity of the system.

To reduce such complexity, the dual-input/dual-output frame band-pass filter is gaining popularity among literature because it does not employ ISC [20]. As a result, many non-ISC BPFs have been identified in the literature. Multiple complex coefficient filters (MCCFs) [21] and $\alpha\beta$-frame DSC [22], [23] are popular non-ISC filters. These BPFs perform better in continuous time-domain FFPS extraction and harmonic removal. However, its digitization in the discrete time domain is problematic and requires high-level mathematical computation. Multiple DSC (MDSC) [24], another class of non-ISC filters, has been reported in the literature to address the discretization issue. It works well enough in nominal frequency cases, however, its effectiveness degrades under the off-nominal frequency cases. The digital signal processing (DSP)-based BPFs [25] and $\alpha\beta$-framed MAF [26] have shown significant performance in extracting the FFPS from distorted and imbalanced three-phase grid conditions. However, their performance deteriorates when the grid operates under off-nominal frequency conditions, where "K" becomes noninteger (if $f_s = Kf_o$', where f_s' is the sampling frequency, f_o' is the nominal frequency, and K is the number of samples in a fundamental time period) [28]. Keeping the view of recent research, it has been established that further effort is required to develop a simple filtering solution with the required features of a good filtering solution such as high rejection ability of harmonics, optimal accuracy, and low computational effort.

In contrast to PLL, frequency estimators can be a better alternative for estimating the fundamental frequency since they avoid nonlinear feedback loops, which offer good dynamic speed. Numerous frequency estimation techniques based on DSP are reported in [29], [30], [31], [32], [33], [34], [35], [36], and [37]. To measure the fundamental frequency, the zero-crossing detector (ZCD) [29] and peak detection method (PDM) [30] are considered simpler and more effective techniques. They perform efficiently with the ideal grid voltage and often produce two zero-crossing points

or voltage peaks in the fundamental cycle. Nevertheless, when harmonically polluted three-phase grid voltage undergoes sudden voltage sag/swell or one-line-drop conditions, false zero-crossings and voltage peaks may emerge in one fundamental cycle, which affects the accuracy of frequency estimation [31]. Moreover, using the DFT [32] and finite-impulse-response (FIR) differentiator filter [33], it is possible to estimate the fundamental frequency. However, it takes a significant amount of careful approximation in implementation. Otherwise, it might lead to instability as regards the digital signal processors, whose impacts are observed in terms of parameter estimation accuracy [34]. Furthermore, the modulation function (MF) technique may be a simple solution for estimating fundamental frequency [35]. Still, MF employs two LPFs in the $\alpha\beta$-frame, which may increase the complexity of the overall system design. Henceforth, the sample storage-based frequency estimation technique is gaining popularity since it provides better accuracy and is easy to implement [37]. Three equidistant samples (3ES) are a straightforward method for estimating the fundamental frequency accurately. However, an issue arises when the instantaneous value of the midterm reaches zero or is close to zero [38]. Establishing a threshold value for the intermediate sample is one possible solution to this issue. Doing so will get rid of any mathematical uncertainty. An enhanced 3ES approach described in [39] improves the performance of the 3ES method. However, its performance deteriorates when sudden changes take place in the grid voltage. Since the frequency estimator alone can handle a selective order of harmonics, the four equidistant sample (4ES)-based technique is gaining popularity in the technical literature [40]. Note that, an additional prefiltering stage is always required to assist the sample-based frequency estimator in achieving better robustness under heavily distorted grid conditions [41]. Despite being a faster dynamic response-based PLL-less solution [41], it ignores the impact of noninteger multiples of harmonics responsible for degrading the power quality. Considering all the above challenges, the present article proposes an improved solution that can accurately estimate grid voltage parameters in the presence of interharmonics and subharmonics. The following are the key features of the proposed PLL-Less approach in contrast to [41]:

1) CBPF is proposed that eliminates the NS and both even and odd-order harmonics.
2) Higher accuracy in estimating fundamental frequency information in the presence of inter/subharmonics under the off-nominal grid voltage conditions.
3) Improved steady-state performance in the estimated parameters in all dynamically worsened grid conditions.

II. THREE-PHASE NONSINUSOIDAL GRID SIGNAL

Apart from PS components, the NS components, the harmonics, and the dc-offset are all examples of disturbances that can be observed in a three-phase practical power system. These disturbances can impact the controller functionality of an inverter-based RES. Hence, taking into account all disturbances, the grid voltage may be expressed as

$$\begin{aligned} v_a(n) &= \sum_{h=1,2,3} \left[V_h^+ \sin\left(\varphi_h^+\right) + V_h^- \sin\left(\varphi_h^-\right)\right] + V_{ao} \\ v_b(n) &= \sum_{h=1,2,3} \left[V_h^+ \sin\left(\varphi_h^+ - \frac{2\pi}{3}\right) + V_h^- \sin\left(\varphi_h^- - \frac{2\pi}{3}\right)\right] + V_{bo} \\ v_c(n) &= \sum_{h=1,2,3} \left[V_h^+ \sin\left(\varphi_h^+ + \frac{2\pi}{3}\right) + V_h^- \sin\left(\varphi_h^- + \frac{2\pi}{3}\right)\right] + V_{co} \end{aligned} \tag{1}$$

where, in (1), $[\varphi_h^+ = hn\omega_g T_s + \phi_h^+]$ and $[\varphi_h^- = -hn\omega_g T_s + \phi_h^-]$. Moreover, $[V_h^+, V_h^-]$, $[\varphi_h^+, \varphi_h^-]$, $(h = 1, 2, 3, \ldots,)$ are the amplitude, phase of the h^{th} harmonic component of the positive and NS of three-phase grid voltage. Moreover, where V_{ao}, V_{bo}, and V_{co} are dc-offset of phase 'a' 'b' and 'c,' respectively. Further, using the Clarke transformation [21], abc-frame voltage can be converted into $\alpha\beta$-frame voltage $v_\alpha(n)$, $v_\beta(n)$ as

$$\begin{aligned} v_\alpha(n) &= \sum_{h=1,2,3,\ldots} \left[\underbrace{V_h^+ \sin\left(\varphi_h^+\right)}_{\text{PS}} + \underbrace{V_h^- \sin\left(\varphi_h^-\right)}_{\text{NS}}\right] + \underbrace{V_{\alpha o}}_{\text{dc-offset}} \\ v_\beta(n) &= \sum_{h=1,2,3,\ldots} \left[\underbrace{V_h^+ \cos\left(\varphi_h^+\right)}_{\text{PS}} + \underbrace{V_h^- \cos\left(\varphi_h^-\right)}_{\text{NS}}\right] + \underbrace{V_{\beta o}}_{\text{dc-offset}} \end{aligned} \tag{2}$$

where $V_{\alpha o} = (2V_{ao} - V_{bo} - V_{co})/3$ and $V_{\beta o} = (V_{bo} - V_{co})/\sqrt{3}$. We may infer that grid disturbances (i.e., NS, harmonics, and dc-offset) in the abc-frame voltage also appear in the $\alpha\beta$-frame voltage under faulty conditions.

III. PROPOSED FREQUENCY ESTIMATION ALGORITHM

It is often desired to have an accurate estimate of the fundamental utility grid frequency in order to control the power converter correctly, thus, a novel FEA has been developed, and its design process is briefly discussed. The effectiveness of the proposed FEA is also evaluated in both the ideal and nonideal grid conditions.

A. DESIGN PROCEDURE UNDER IDEAL THREE-PHASE SINUSOIDAL CONDITION

Considering the ideal three-phase grid voltage contains an FFPS can be represented as

$$\begin{aligned} v_{\alpha,1}^+(n) &= V_1^+ \sin\left(n\omega_g T_s + \phi_1^+\right) \\ v_{\beta,1}^+(n) &= V_1^+ \cos\left(n\omega_g T_s + \phi_1^+\right). \end{aligned} \tag{3}$$

In practice, a sudden turn-on or turn-off of a heavy load can cause voltage sags and swells in the grid voltage, negatively affecting the transient process of FEA. The normalization process is recommended in [43] to mitigate such negative impacts as

$$S_{\alpha,1}(n) = v_{\alpha,1}^+(n)/A;\ S_{\beta,1}(n) = v_{\beta,1}^+(n)/A \tag{4}$$

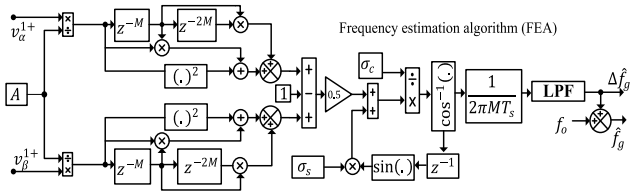

FIGURE 1. Proposed FEA.

where $A = \sqrt{(v^+_{\alpha,1}(n))^2 + (v^+_{\beta,1}(n))^2}$, and $S_{\alpha,1}(n)$ and $S_{\beta,1}(n)$ are the normalized fictitious voltage samples. Moreover, $S_{\alpha,2}(n)$, $S_{\beta,2}(n)$, and $S_{\alpha,3}(n)$, $S_{\beta,3}(n)$ are derived from the $S_{\alpha,1}(n)$, $S_{\beta,1}(n)$, by delaying the "M" and "$2M$" sample, respectively. Further, using the fictitious voltage samples $S_{\alpha,1}(n)$, $S_{\beta,1}(n)$, $S_{\alpha,2}(n)$, $S_{\beta,2}(n)$, and $S_{\alpha,3}(n)$, $S_{\beta,3}(n)$, the intermediate voltage signals U_α and U_β can be framed as

$$U_\alpha = S_{\alpha,1}(n)S_{\alpha,2}(n) + \left[S_{\alpha,1}(n)\right]^2 + S_{\alpha,2}(n)S_{\alpha,3}(n) \quad (5)$$

$$U_\beta = S_{\beta,1}(n)S_{\beta,2}(n) + \left[S_{\beta,1}(n)\right]^2 + S_{\beta,2}(n)S_{\beta,3}(n). \quad (6)$$

Further (5) and (6) can be simplified as

$$U_\alpha = \left[S_{\alpha,1}(n)\right]^2\left(1+\cos\left(M\omega_g T_s\right)\right) + \left[S_{\alpha,2}(n)\right]^2\cos\left(M\omega_g T_s\right) - \sin\left(M\omega_g T_s\right)\left[S_{\alpha,1}(n)S_{\beta,1}(n) + S_{\alpha,2}(n)S_{\beta,2}(n)\right] \quad (7)$$

$$U_\beta = \left[S_{\beta,1}(n)\right]^2\left(1+\cos\left(M\omega_g T_s\right)\right) + \left[S_{\beta,2}(n)\right]^2\cos\left(M\omega_g T_s\right) + \sin\left(M\omega_g T_s\right)\left[S_{\beta,1}(n)S_{\alpha,1}(n) + S_{\beta,2}(n)S_{\alpha,2}(n)\right]. \quad (8)$$

Adding (7) and (8), one may obtain as

$$\cos\left(M\omega_g T_s\right) = \frac{1}{2}\left(U_\alpha + U_\beta - 1\right). \quad (9)$$

As instantaneous grid fundamental frequency is the sum of nominal frequency (f_o) and deviation of frequency from nominal one ($\Delta\hat{f}_g$), i.e., $\hat{f}_g = f_o + \Delta\hat{f}_g$. Therefore, (9) can be further rewritten as

$$\cos\left(2\pi\left(f_o + \Delta\hat{f}_g\right)MT_s\right) = \frac{1}{2}\left(U_\alpha + U_\beta - 1\right). \quad (10)$$

The extended form of (10) is as follows:

$$\sigma_c \cos\left(2\pi\,\Delta\hat{f}_g MT_s\right) - \sigma_s \sin\left(2\pi\,\Delta\hat{f}_g MT_s\right) = U \quad (11)$$

where $U = \frac{1}{2}(U_\alpha + U_\beta - 1)$, and $\sigma_c = \cos(2\pi f_o MT_s)$ and $\sigma_s = \sin(2\pi f_o MT_s)$ are represented as the constant terms. Now, deviation in frequency can be defined as

$$\Delta\hat{f}_g = \frac{1}{2\pi MT_s}\cos^{-1}\left[\frac{U + \sigma_s \sin\left(2\pi\,\Delta\hat{f}_g MT_s\right)}{\sigma_c}\right]. \quad (12)$$

In order to make the (12) digitally realizable, it can be further written as

$$\Delta\hat{f}_g(n) = \frac{1}{2\pi MT_s}\cos^{-1}\left[\frac{U + \sigma_s \sin\left(2\pi\,\Delta\hat{f}_g(n-1)MT_s\right)}{\sigma_c}\right]. \quad (13)$$

As (13), the proposed FEA technique depends on selecting an optimal value of parameter M shown in Fig. 1. A lower value of M implies the technique is more vulnerable to noise, which can introduce inaccuracies in the estimated value of $\Delta\hat{f}_g$. Conversely, a higher value of 'M' leads to slower dynamic performance. To evaluate the performance of the proposed FEA, the Gaussian noise is added to the FFPS component (refer to expression 1) of the grid voltage, as follows:

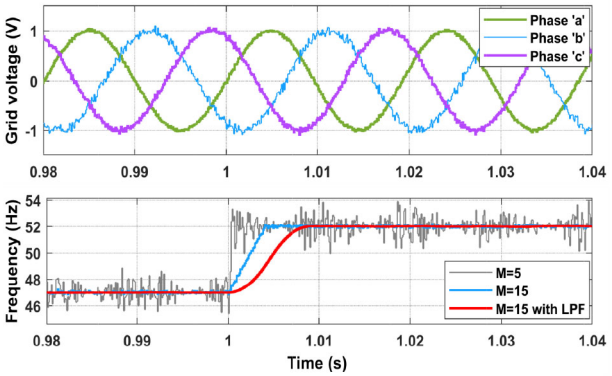

FIGURE 2. Selection of suitable value of "M" for FEA.

$$\begin{aligned} v_{a(\text{noisy})}(n) &= V_1^+ \sin\left(\varphi_1^+\right) + \mathcal{N}\left(0, \sigma_a^2\right) \\ v_{b(\text{noisy})}(n) &= V_1^+ \sin\left(\varphi_1^+ - \frac{2\pi}{3}\right) + \mathcal{N}\left(0, \sigma_b^2\right) \\ v_{c(\text{noisy})}(n) &= V_1^+ \sin\left(\varphi_1^+ + \frac{2\pi}{3}\right) + \mathcal{N}\left(0, \sigma_c^2\right). \end{aligned} \quad (14)$$

Here, $\mathcal{N}(0, \sigma_a^2)$, $\mathcal{N}(0, \sigma_b^2)$, and $\mathcal{N}(0, \sigma_c^2)$ represent the Gaussian noise with zero mean and variances of σ_a^2, σ_b^2 and σ_c^2, respectively. We specify the desired variances σ_a^2, σ_b^2, and σ_c^2 for the noise to achieve the desired SNR levels of 25 dB in phase "a," 30 dB in phase "b," and 35 dB in phase "c." These noise levels are introduced when the fundamental frequency drifts of 5 Hz (47–52 Hz), as specified in the EN50160 standard [44]. Thus, Fig. 2, illustrates that the smaller value of M is incapable of entirely eliminating noise that is present in the input signal, and consequently, fails to estimate the fundamental frequency accurately. Furthermore, $M = 15$, with the LPF (window length $T_w = T_o/4$; where $T_o = 1/f_o$; f_o is the nominal frequency of the grid voltage), performs well, is minimally impacted by noise, and effectively determines the fundamental frequency of the polluted grid voltage signal.

B. FREQUENCY ESTIMATION ALGORITHM UNDER NONIDEAL CONDITION

Despite the fact that three-phase grid voltage is not ideal in practice, dc-offset is combined with FFPS components in this case. Since CT prevents equal dc-offset, the grid voltage is held responsible for the unequal dc-offset. On account of this, it could be expressed as

$$\begin{aligned} v_\alpha(n) &= V_1^+ \sin\left(n\omega_g T_s + \phi_1^+\right) + V_{\alpha o} \\ v_\beta(n) &= V_1^+ \cos\left(n\omega_g T_s + \phi_1^+\right) + V_{\beta o}. \end{aligned} \quad (15)$$

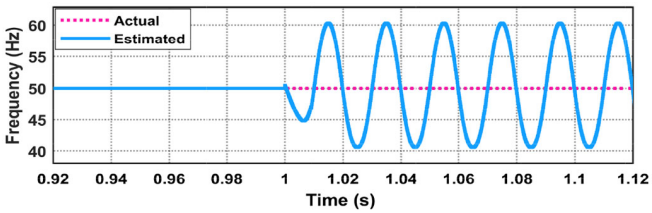

FIGURE 3. Estimation of fundamental frequency under dc-offset.

Using normalization process the following can be obtained as:

$$S^*_{\alpha 1}(n) = \frac{v_\alpha(n)}{A^*} = V^* \sin\left(n\omega_g T_s + \phi_1^+\right) + V^*_{\alpha o} \tag{16}$$

$$S^*_{\beta 1}(n) = \frac{v_\beta(n)}{A^*} = V^* \cos\left(n\omega_g T_s + \phi_1^+\right) + V^*_{\beta o} \tag{17}$$

$$\text{where } A^* = \sqrt{(v_\alpha)^2 + \left(v_\beta\right)^2} = \sqrt{\underbrace{\left(V_1^+\right)^2 + \left(V_{\beta o}\right)^2 + (V_{\alpha o})^2}_{\text{constant term}} + \underbrace{2V_1^+ G_1(n)}_{\text{oscillatory term}}} \tag{18}$$

where $G_1(n) = V_{\alpha o}\sin(n\omega_g T_s + \phi_1^+) + V_{\beta o}\cos(n\omega_g T_s + \phi_1^+)$. Further, intermediate voltage term can be defined as

$$U^*_\alpha = S^*_{\alpha,1}(n)S^*_{\alpha,2}(n) + \left[S^*_{\alpha,1}(n)\right]^2 + S^*_{\alpha,2}(n)S^*_{\alpha,3}(n) \tag{19}$$

$$U^*_\beta = S^*_{\beta,1}(n)S^*_{\beta,2}(n) + \left[S^*_{\beta,1}(n)\right]^2 + S^*_{\beta,2}(n)S^*_{\beta,3}(n). \tag{20}$$

After simplifying the (20), and (21) we get

$$\left(V^*\right)^2\left[1 + 2\cos M\omega_g T_s\right] + G_2(n) = U^*_\alpha + U^*_\beta \tag{21}$$

where $G_2(n) = V^*_{\alpha o}[3S^*_{\alpha,1}(n) + 2S^*_{\alpha,2}(n) + S^*_{\alpha,3}(n) - 3V^*_{\alpha o}] + V^*_{\beta o}[3S^*_{\beta,1}(n) + 2S^*_{\beta,2}(n) + S^*_{\beta,3}(n) - 3V^*_{\beta o}]$. Further, following the steps from the previous section, the deviation in frequency can be defined as:

$$\Delta\hat{f}_g(n) = \frac{1}{2\pi MT_s}\cos^{-1}\left[\frac{U^* + \sigma_s \sin\left(2\pi\,\Delta\hat{f}_g(n-1)MT_s\right)}{\sigma_c}\right] \tag{22}$$

where $U^* = 0.5[(U^*_\alpha + U^*_\beta - G_2(n))/(V^*)^2 - 1]$. From (22), it can be observed that due to the dc-offset $(V_{\alpha o}, V_{\beta o})$, the FEA involves the extra oscillatory terms $G_2(n)$ and $(V^*)^2$, which leads to oscillations in the fundamental frequency (Fig. 3). Similarly, when considering a more real scenario during abnormalities, the grid voltage is commonly polluted with NS and harmonics, which may raise the oscillations in the proposed FEA. As a result, a prefiltering technique is combined with the proposed FEA to mitigate this effect. In light of the aforementioned issue, a prefilter is proposed in this work and is discussed in the following section.

C. ELIMINATION OF DC-OFFSET AND EVEN-ORDER HARMONICS

As demonstrated previously, the existence of dc-offset in a three-phase utility grid voltage signal has a negative impact on the FEA and, as a result, performance degrades. Thus, a BPF is intended to primarily act as a harmonic blocker and can efficiently remove the dc-offset to enhance the overall performance of the FEA. To clarify the action plan, a well-known LPF is regarded as an initial step in this process and can be expressed as

$$H_L(s) = \frac{\omega_c}{s + \omega_c} \tag{23}$$

where the cut-off frequency of $H_L(s)$ is considered as 'ω_c'. Now, translating the center frequency at nominal value, i.e., $(s - j\omega_o)$; $\omega_o = 2\pi f_o$, the low-pass characteristics transform into band-pass, can be represented as

$$H_B(s) = \frac{\omega_c}{s + (\omega_c - j\omega_o)}. \tag{24}$$

For the discrete frequency-domain design of (24), the continuous poles of BPF are mapped into discrete poles considering the $z_p = e^{s_p T_s}$. Hence, (24) can be written as

$$H_B(z) = \frac{G}{\left[1 - \lambda(\sigma + j\rho)z^{-1}\right]} \tag{25}$$

where "G" in (25) is the transformation gain factor, $\lambda = e^{-\omega_c T_s}$ and $\sigma + j\rho = \cos(\omega_o T_s) + j\sin(\omega_o T_s) = e^{j\omega_o T_s}$. Further, using magnitude normalization from s-domain to z-domain at nominal frequency, i.e., $z = e^{j\omega_o T_s}$, the value of G can be calculated as

$$H_B(z = e^{j\omega_o T_s}) = 1 \qquad G = 1 - \lambda. \tag{26}$$

Therefore, one may write for the case when G is substituted in (25) as follows:

$$H_B(z) = \frac{(1-\lambda)}{\left[1 - \lambda(\sigma + j\rho)z^{-1}\right]}. \tag{27}$$

The frequency response of (27) has been shown in Fig. 4. It is quite obvious that even after employing a conventional BPF, the elimination of dc-bias is impossible. Therefore, thanks to the comb filter (CF), which readily eliminates the even-order harmonics and DC-offset, and as such utilized in this work and is expressed by the following transfer function:

$$H_C(z) = \frac{1}{2}\left[1 - z^{-\frac{N}{2}}\right] \tag{28}$$

where $N = \frac{f_s}{f_o}$ (f_s and f_o are the sampling frequency and nominal frequency in Hz). Moreover, the cascading of the CF with BPF can provide the excellent rejection of dc-offset and even-order harmonics. Therefore, the cascading of CF and BPF can be written as

$$H_{B1}(z) = H_B(z).H_C(z) = \frac{(1/2)\left(1 - z^{-\frac{N}{2}}\right)(1-\lambda)}{\left[1 - \lambda(\sigma + j\rho)z^{-1}\right]}. \tag{29}$$

Considering that the input and output voltage are in complex forms. Therefore, (29) can be expressed as

$$\frac{V_{\alpha(B1)}(z) + jV_{\beta(B1)}(z)}{V_\alpha(z) + jV_\beta(z)} = \frac{(1/2)\left(1 - z^{-\frac{N}{2}}\right)(1-\lambda)}{\left[1 - \lambda(\sigma + j\rho)z^{-1}\right]} \tag{30}$$

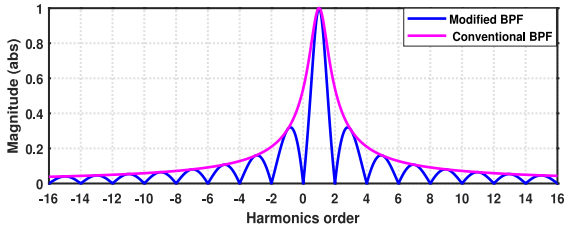

FIGURE 4. Frequency response plot of $H_{B1}(z)$.

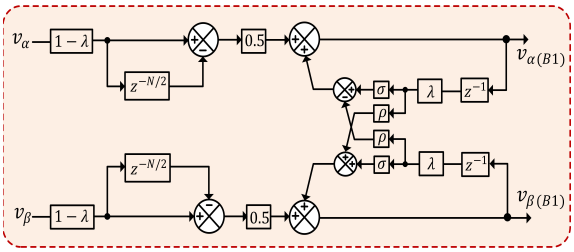

FIGURE 5. Digital implementation of $H_{B1}(z)$.

where $V_{\alpha(B1)}(z)$, $V_{\beta(B2)}(z)$ and $V_\alpha(z)$, $V_\beta(z)$ are the output and input voltage of $H_{B1}(z)$ in $\alpha\beta$-frame, respectively. Now, segregating the real and imaginary pairs (30) as

$$V_{\alpha(B1)}(z) - \lambda\left[\sigma V_{\alpha(B1)}(z)z^{-1} - \rho V_{\beta(B1)}(z)z^{-1}\right] = \frac{1}{2}(1-\lambda)\left(1 - z^{-\frac{N}{2}}\right)V_\alpha(z) \tag{31}$$

$$V_{\beta(B1)}(z) - \lambda\left[\sigma V_{\beta(B1)}(z)z^{-1} + \rho V_{\alpha(B1)}(z)z^{-1}\right] = \frac{1}{2}(1-\lambda)\left(1 - z^{-\frac{N}{2}}\right)V_\beta(z). \tag{32}$$

The straightforward inverse z-transform can be used to obtain the time domain expression of (31) & (32) as

$$v_{\alpha(B1)}(n) = \frac{1}{2}(\lambda-1)\left[v_\alpha(n) - v_\alpha\left(n - \frac{N}{2}\right)\right] + \lambda\left[\sigma v_{\alpha(B1)}(n-1) - \rho v_{\beta(B1)}(n-1)\right]. \tag{33}$$

Similarly, the imaginary part of the proposed BPF is

$$v_{\beta(B1)}(n) = \frac{1}{2}(\lambda-1)\left[v_\beta(n) - v_\beta\left(n - \frac{N}{2}\right)\right] + \lambda\left[\sigma v_{\beta(B1)}(n-1) + \rho v_{\alpha(B1)}(n-1)\right]. \tag{34}$$

Using (33) and (34), digital implementation of modified BPF is straightforward, as seen in Fig. 5. There is less mathematical computation needed for digital implementation. Fig. 4, depicts the frequency response graph of the improved BPF. The improved BPF eliminates the dc-offset (0 Hz) and even-harmonics "$2hf_o$"; $h = \pm1, \pm2, \pm3, \ldots,$ to the aliasing point.

D. ELIMINATION OF FUNDAMENTAL FREQUENCY NEGATIVE SEQUENCE COMPONENT AND ODD-ORDER HARMONICS

As discussed, the immunity against the even-order harmonics and the dc-offset is possible with the employment of the previously suggested BPF. However, the odd-order harmonics are still present in the output of $H_{B1}(z)$. Thus, to resolve this problem another half-cycle LPF is incorporated which not only targets the elimination of odd-harmonics but the fundamental frequency NS (FFNS). The transfer function of LPF is expressed as [46]

$$H_2(z) = \Gamma \sum_{l=0}^{l=\frac{N}{2}-1} z^{-l}. \tag{35}$$

Herein, N denotes the no of samples in one fundamental cycle. The term Γ is considered the filter coefficient. Now, using simple geometric series, the sum of $N/2$ terms can be defined as

$$H_2(z) = \frac{\Gamma\left(1 - z^{-\frac{N}{2}}\right)}{(1 - z^{-1})}. \tag{36}$$

By using frequency translation, the ω_o is assigned to the center frequency, i.e., $z \to ze^{-j\omega_o T_s}$ and the modified form of (36) is

$$H_{B2}(z) = \frac{\Gamma\left[1 - \left(ze^{-j\omega_0 T_s}\right)^{-\frac{N}{2}}\right]}{\left[1 - (ze^{-j\omega_0 T_s})^{-1}\right]} = \frac{\Gamma\left[1 - (\sigma_1 + j\rho_1)z^{-\frac{N}{2}}\right]}{\left[1 - (\sigma + j\rho)z^{-1}\right]} \tag{37}$$

where $e^{j\omega_o T_s \frac{N}{2}} = \cos(\omega_o T_s \frac{N}{2}) + j\sin(\omega_o T_s \frac{N}{2}) = \sigma_1 + j\rho_1$. The most significant characteristic of the BPF is amplitude versus frequency response. To achieve the ideal filtering qualities, unity magnitude at the tuned frequency is required

$$\left|H_{B2}(z)\right|_{\omega=\omega_o} = \left|\frac{\Gamma\left[1 - (\sigma_1 + j\rho_1)z^{-\frac{N}{2}}\right]}{\left[1 - (\sigma + j\rho)z^{-1}\right]}\right|_{\omega=\omega_o} = 1$$

$$\Gamma = \frac{2T_s}{T_o}. \tag{38}$$

Considering that the complex output and input are involved in $H_{B2}(z)$, it can be expressed as follows:

$$\frac{V_{\alpha(B2)}(z) + jV_{\beta(B2)}(z)}{V_{\alpha(B1)}(z) + jV_{\beta(B1)}(z)} = \frac{\left(\frac{2T_s}{T_o}\right)\left[1 - (\sigma_1 + j\rho_1)z^{-\frac{N}{2}}\right]}{\left[1 - (\sigma + j\rho)z^{-1}\right]}. \tag{39}$$

Further (39), can be simplified as

$$V_{\alpha(B2)}(z) - z^{-1}\left[\sigma V_{\alpha(B2)}(z) - \rho V_{\beta(B2)}(z)\right]$$

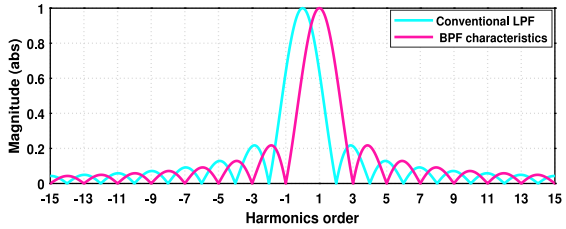

FIGURE 6. Frequency response of $H_{B2}(z)$.

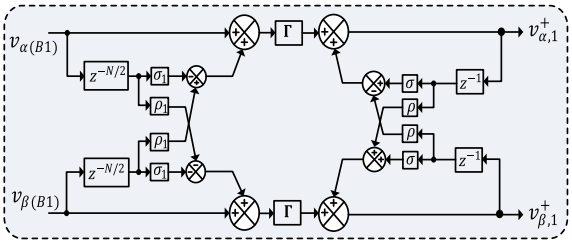

FIGURE 7. Digital implementation of $H_{B2}(z)$.

$$= V_{\alpha(B1)}(z) - z^{-\frac{N}{2}}\left[\sigma_1 V_{\alpha(B1)}(z) - \rho_1 V_{\beta(B1)}(z)\right]\left(\frac{2T_s}{T_o}\right) \quad (40)$$

$$V_{\beta(B2)}(z) - z^{-1}\left[\sigma V_{\beta(B2)}(z) + \rho V_{\alpha(B2)}(z)\right]$$

$$= V_{\beta(B1)}(z) - z^{-\frac{N}{2}}\left[\sigma_1 V_{\beta(B1)}(z) + \rho_1 V_{\alpha(B1)}(z)\right]\left(\frac{2T_s}{T_o}\right). \quad (41)$$

To invert (40) and (41) from frequency domain to time domain, we consider the Fourier transforms $V_{\alpha(B2)}(z), V_{\beta(B2)}(z) \leftrightarrow v_{\alpha(B2)}(n), v_{\beta(B2)}(n) = v^+_{\alpha,1}(n), v^+_{\beta,1}(n)$. Thus, it can express the FFPS $[v^+_{\alpha,1}(n)$ and $v^+_{\beta,1}(n)]$ in the time domain as

$$v^+_{\alpha,1}(n) = \left(\frac{2T_s}{T_o}\right)\left[v_{\alpha(B1)}(n) - \sigma_1 v_{\alpha(B1)}\left(n - \frac{N}{2}\right) + \rho_1 v_{\beta(B1)}\left(n - \frac{N}{2}\right) + \sigma v^+_{\alpha,1}(n-1) - \rho v^+_{\beta,1}(n-1)\right] \quad (42)$$

$$v^+_{\beta,1}(n) = \left(\frac{2T_s}{T_o}\right)\left[v_{\beta(B1)}(n) - \sigma_1 v_{\beta(B1)}\left(n - \frac{N}{2}\right) - \rho_1 v_{\alpha(B1)}\left(n - \frac{N}{2}\right) + \sigma v^+_{\beta,1}(n-1) + \rho v^+_{\alpha,1}(n-1)\right]. \quad (43)$$

Fig. 6, shows the frequency response plot of the expression (37) (a). From there, it is obvious that the newly designed BPF completely eliminates the odd-order harmonics $(2h+1)f_o$; $h = \pm1, \pm2, \pm3, \ldots$, including FFNS $(-50$ Hz). Moreover, employing (42) and (43) as mathematical models for the digital implementation is illustrated in Fig. 7, which is straightforward to execute.

E. COMBINED BAND-PASS FILTER

The crucial unwanted components, i.e., the dc-offset (0 Hz), the FFNS (-50 Hz), and the even-order $(2hf_o)$ cum odd-order $((2h+1)f_o)$ harmonics must be rejected rapidly such that the parameter detection is precisely done by grid synchronization

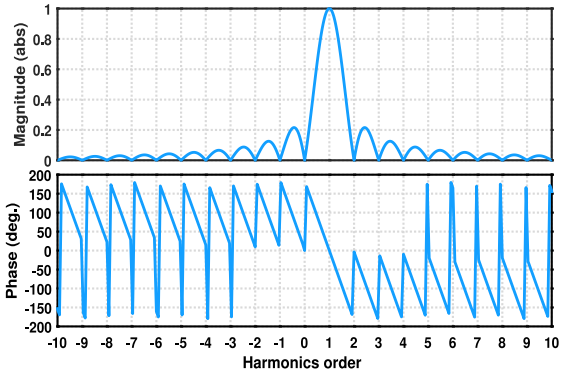

FIGURE 8. Frequency response plot of $H_p(z)$.

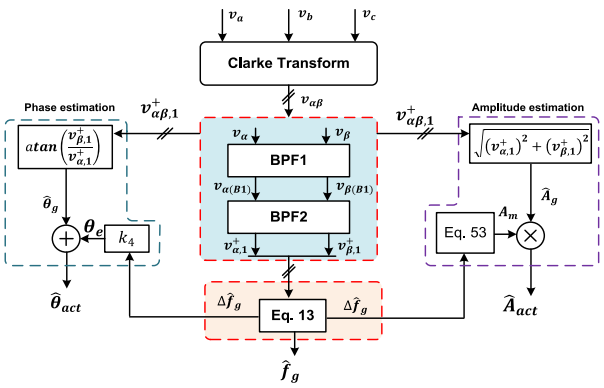

FIGURE 9. Block diagram of the proposed three-phase CBPF-based grid variables detection approach.

techniques. Thus, accurate and fast computation of FFPS is ensured by cascading the modified BPF with a conventional LPF, whose transfer function is given below

$$H_p(z) = H_{B1}(z)H_{B2}(z) = \frac{(1-\lambda)\left(\frac{2T_s}{T_o}\right)\left[1 - z^{-\frac{N}{2}}\right]\left[1 - (\sigma_1 + j\rho_1)z^{\frac{-N}{2}}\right]}{\left[1 - \lambda(\sigma + j\rho)z^{-1}\right]\left[1 - (\sigma + j\rho)z^{-1}\right]} \quad (44)$$

where $H_p(z)$ is referenced by a combined prefilter but precisely described as "prefiltering approach." The frequency response of the $H_p(z)$ is shown in Fig. 8, which suppresses the dc-offset, FFNS, and harmonics and allows only the FFPS with unity amplitude and no phase shift.

IV. PHASE-ANGLE AND AMPLITUDE ERROR-RESOLVING APPROACH

The nonadaptive nature of $H_p(z)$ can result in incorrect amplitude and phase information when the grid operates at off-nominal frequencies. To address this issue, an error correction block can be integrated into the proposed technique to rescue from erroneous estimations. Note that, the transfer function of the $H_p(z)$ is frequency-dependent, it can be used to define the frequency-dependent error

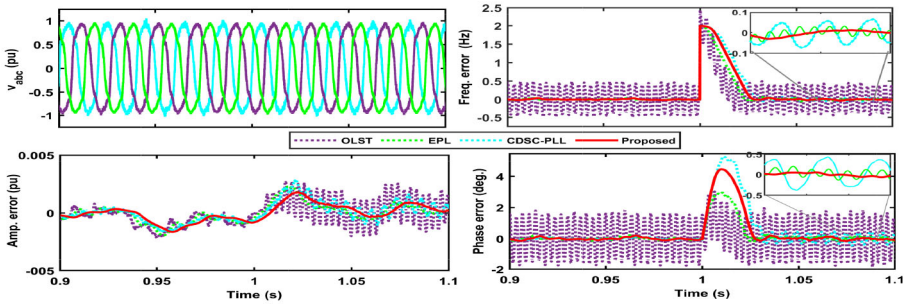

FIGURE 10. Transient and steady-state accuracy assessment of the estimated parameters in the presence of Gaussian white noise and harmonics.

TABLE 1. Control parameters and assessment of processing burden.

Schemes (↓)	Control Prameters (↓)	Processor Burden			
		+/-	×/÷	SQRT	T IT
OLST [42]	FEA: $\omega_n = 2\pi 50r/s, T_s = 0.0001s$, pre-filtering: $T_w = 0.02s$	20	25	2	2 1
EPL [41]	FEA: $N_f = 50, T_s = 0.0001s$ Pre-filtering: $N = 200, T_o = 0.02s, p = 1$	18	22	1	2 2
CDSC-PLL [23]	PLL: $k_p = 188, k_\phi = 0.0125$ Pre-filtering: $T_w = T/4, T = 0.02s$	30	32	1	2 1
Proposed	FEA: $M = 15, T_s = 0.0001s$ Pre-filtering: $N_{B1} = 100, N_{B2} = 100$	22	24	1	2 2

*SQRT–square root **Mathematical Functions: T–trigonometry and IT–inverse trigonometry

correction factors. Now, substituting $z = e^{j2\pi f_g T_s}$ in (46) as follows:

$$H_p(z)\Big|_{z=e^{j2\pi f_g T_s}} = H_p(f_g) = e^{-j\left[2\pi\left(f_g - f_o\right)\left(\frac{T_o}{4} - \frac{T_s}{2}\right) + \frac{f_g T_o}{4}\right) - \frac{\pi}{2}]} \times \frac{2\sin\left(\frac{\pi f_g T_o}{2}\right)\sin\left(\frac{\pi(f_g - f_o)T_o}{2}\right)}{\sin\left(\pi(f_g - f_o)T_s\right)}. \quad (45)$$

Now, defining $f_g = f_o + \Delta f_g$ in (45), one may obtain

$$H_p(f_g) = e^{-j[\pi\,\Delta f_g(T_o - T_s)]} \cdot \frac{2\cos\left(\frac{\pi\,\Delta f_g T_o}{2}\right)\sin\left(\frac{\pi\,\Delta f_g T_o}{2}\right)}{\sin\left(\pi\,\Delta f_g T_s\right)}. \quad (46)$$

The amplitude factor from (46) can be defined as

$$\left|H_p(f_g)\right| = \left|\frac{2\cos\left(\frac{\pi\,\Delta f_g T_o}{2}\right)\sin\left(\frac{\pi\,\Delta f_g T_o}{2}\right)}{\sin\left(\pi\,\Delta f_g T_s\right)}\right|. \quad (47)$$

In order to avoid the additional trigonometric function in (47), the Taylor series expansion can be utilized, providing

$$\frac{1}{N}\left|H_p(f_g)\right| \approx \left|\frac{1 - (k_1 + k_2)(\Delta f_g)^2 + k_1 k_2 (\Delta f_g)^4}{1 - k_3(\Delta f_g)^2}\right| \quad (48)$$

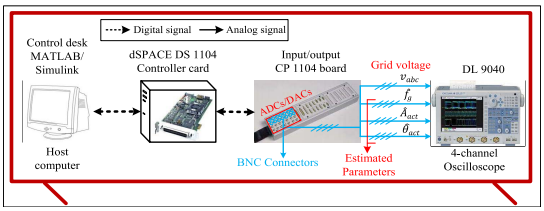

FIGURE 11. Prototype hardware setup for conducting experiments.

where $k_1 = (\frac{\pi T_o}{2})^2$, $k_2 = (\frac{\pi T_s}{2})^2$, and $k_3 = \frac{\pi^2 T_s^2}{2}$ are constant terms. To further elaborate on the phase factor described in (46), it can be expressed in terms of grid frequency

$$\angle H_p(f_g) = -\pi T_o \Delta f_g + \pi T_s \Delta f_g. \quad (49)$$

Since expression (49) allows us to rewrite it in linear form in terms of Δf_g, it can be expressed as

$$\underbrace{-\angle H_p(f_g)}_{\theta_e} \approx k_4 \Delta f_g \quad (50)$$

where the constant term is denoted by $k_4 = \pi(T_o - T_s)$, which is independent of the frequency. It is noteworthy that at $f_g = f_o$, (50) yields zero. However, if the frequency varies, it acts as a rescuer for the phase estimator, providing the correct phase angle value. From [38], [39], and [41], the grid voltage amplitude, $(\hat{A}_g)$ can be estimated as

$$\hat{A_g} = \sqrt{\left(v^+_{\alpha,1}\right)^2 + \left(v^+_{\beta,1}\right)^2}. \quad (51)$$

At nominal conditions, the magnitude in the output of $|H_{(p)}(z)|$ is unity, indicating that $\hat{A}_g$ being equal to the actual grid voltage amplitude $(\hat{A}_{\text{act}})$. However, if the grid frequency deviates from its nominal value, $\hat{A}_g$ will not be equal to $\hat{A}_{\text{act}}$, and an amplitude multiplication factor (A_m) is needed which is obtained by rearranging (50) as explained in the subsequent steps

$$\hat{A}_{\text{act}} \approx \left(A_m\right) \cdot \hat{A}_g \quad (52)$$

where A_m is given below

$$\left(A_m\right) \approx \left|\frac{1 - k_3(\Delta f_g)^2}{1 - (k_1 + k_2)(\Delta f_g)^2 + k_1 k_2 (\Delta f_g)^4}\right|. \quad (53)$$

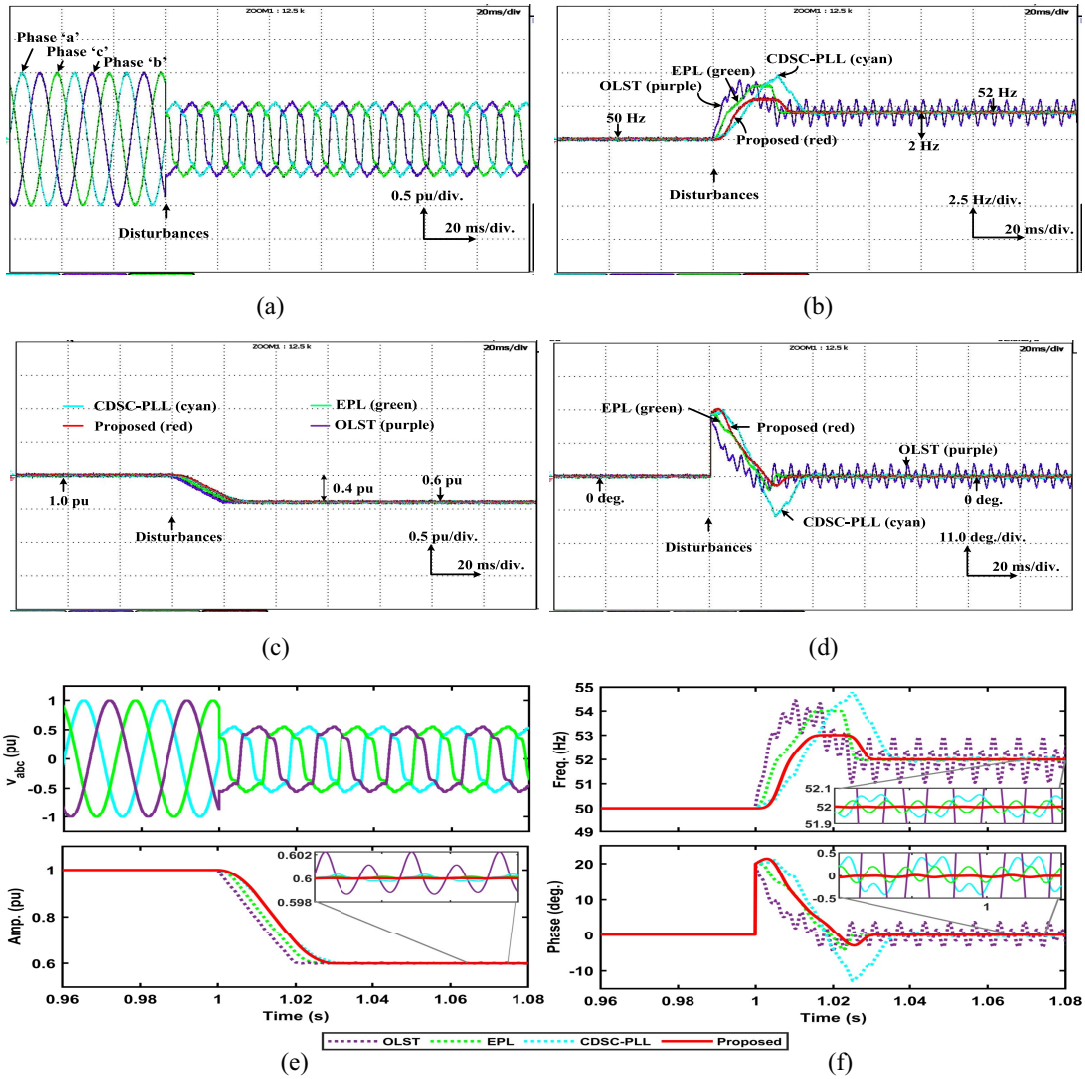

FIGURE 12. Test study S-1: experimental [12(a)–(d)] and simulation results [12(e)] in the presence of phase jump (20°), voltage sag (50%), frequency step (50-52 Hz), and harmonic disturbances (Table 2). (a) Three-phase grid voltage. (b) Estimated fundamental frequency ($\hat{f}_g$). (c) Estimated actual amplitude ($\hat{A}_{\text{act}}$). (d) Estimated actual phase-angle ($\hat{\theta}_{\text{act}}$). (e) Simulation results of estimated parameters under nonideal grid voltage conditions.

The Δf_g is the difference between the actual grid frequency and the nominal frequency. On the other hand, the estimation of the instantaneous actual phase angle of the utility grid is computed as follows:

$$\hat{\theta}_{\text{act}} = \hat{\theta}_g + \theta_e \tag{54}$$

where $\hat{\theta}_g$ is the estimated phase-angle using the arctangent function and θ_e is the phase-angle error correction term and $\hat{\theta}_g$ is calculated by utilizing the FFPS components as

$$\hat{\theta}_g = \tan^{-1}\left(\frac{v^+_{\beta,1}}{v^+_{\alpha,1}}\right). \tag{55}$$

To correct the phase-angle under frequency deviations, the frequency-dependent θ_e is required, which has a linear relationship with $\Delta\hat{f}_g$ also obtained from (50). From the relationship shown in (54), the adaptive nature of $\hat{\theta}_{\text{act}}$ is confirmed. Furthermore, the block diagram illustrated in Fig. 9 represents the workflow of the proposed technique used for estimating the fundamental amplitude, frequency, and phase-angle in three-phase applications.

V. NOISE SENSITIVITY ANALYSIS WITH HARMONICS

Within the dynamic framework of power grid, characterized by various uncertainties, therefore, accurate measurement of error in the estimated parameter is vital for seamless power converter integration. To assess the uncertainty in grid voltage, and hence verify the efficacy of the proposed scheme, harmonics are taken into account, as outlined in Table 2, which reports a total harmonic distortion (THD) of 15.32% accordance with the EN-50160 standard [44]. This assessment is further enriched by the inclusion of noise at 25, 30, and 35 dB, under the frequency drift of +2 Hz from 50 to 52 Hz. The techniques under consideration include advanced PLL and PLL-Less techniques, such as cascaded DSC-based PLL (CDSC-PLL) [23], the enhanced PLL-less

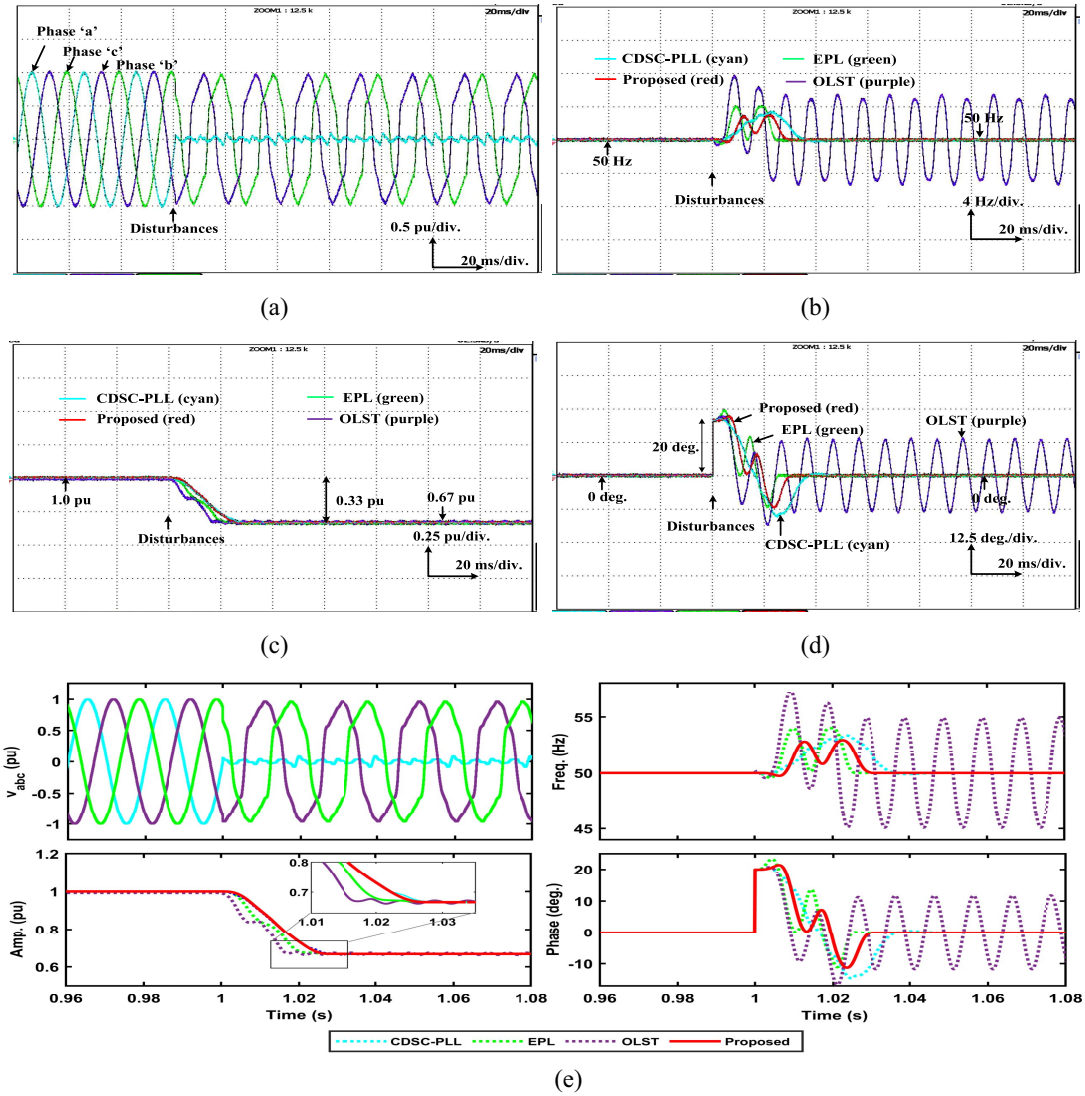

FIGURE 13. Test study S-2: experimental [13(a)–(d)] and simulation results [13(e)] in the presence of FNS (0.33 pu), phase jump (20°), and harmonic disturbances (Table 2). (a) Three-phase grid voltage ($\hat{f}_g$). (b) Estimated fundamental frequency. (c) Estimated actual amplitude ($\hat{A}_{act}$). (d) Estimated actual phase-angle ($\hat{\theta}_{act}$). (e) Simulation results of S-2.

technique (EPL) [41] and the simple and popular open-loop synchronization technique (OLST) [42]. The control parameters of each method are detailed in Table 1. Fig. 10 presented herein offers a comprehensive comparison of the errors yielded by various methods, elucidating relative error (RE %) in steady-state grid voltage parameters

$$\text{RE}(\%) = \left| \frac{\text{Actual value - Estimated value}}{\text{Actual value}} \right| \times 100. \quad (56)$$

Specifically, in terms of frequency, CDSC-PLL exhibits a 0.11% error, OLST records 0.96%, EPL demonstrates 0.076%, and the proposed method achieves an impressive 0.03% error which is under the limit mentioned in the grid code IEC standard 61000-4-7 [45]. Similarly, for phase-angle estimation, CDSC-PLL reports a 0.4° error, OLST records 1.8°, EPL shows 0.2°, and the proposed approach attains a minimal 0.06° error. Furthermore, in amplitude estimation, CDSC-PLL, OLST, and EPL exhibit 0.12%, 0.25%, and 0.15% errors, respectively, while the proposed method outshines with a 0.04% error. The numerical findings support the proposed scheme's superior performance compared to other methods that can address the uncertainties of grid voltage dynamics.

VI. SIMULATION AND EXPERIMENTAL RESULT

Using the experimental test bench depicted in Fig. 11, the early validation of the current proposal is discussed. An efficient real-time controller, i.e., dSPACE (DS1104), compatible with the MATLAB/Simulink environment, is utilized for the hassle-free code generation of the proposed synchronization algorithm. The simulation environment constructed in MATLAB/Simulink uses a fixed step mode and 10 kHz sampling frequency. Note that, the input signal is synthetically generated within the controller to develop a three-phase grid voltage signal in the range of 1 V and is treated as 1 pu signal, later sent to the real world

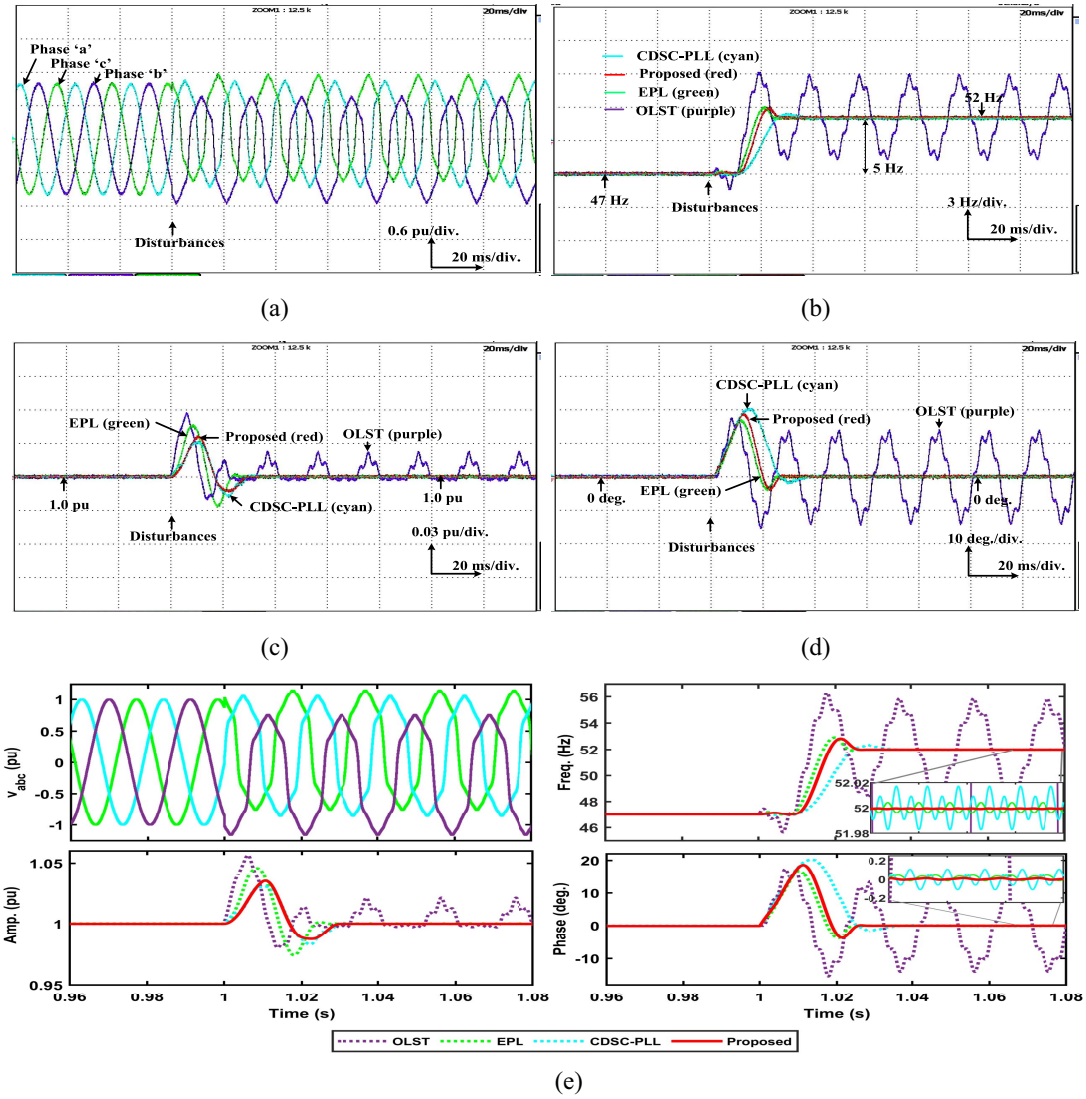

FIGURE 14. Test study S-3: experimental [14(a)–(d)] and simulation results [14(e)] in the presence of dc-offset (10% in phase "a", -20% in phase "b" and +20% in phase "c"), frequency drift of 5 Hz (47 –52 Hz) and harmonic disturbances (Table 2). (a) Three-phase grid voltage. (b) Estimated fundamental frequency ($\hat{f}_g$). (c) Estimated actual amplitude ($\hat{A}_{act}$). (d) Estimated actual phase-angle ($\hat{\theta}_{act}$). (e) Simulation results of S-3.

using the digital-to-analog converter (DAC) ports of the CLP-1104 board using the three-BNC connector cables. This process helps early verification of the synchronization algorithms and avoids using costly programmable power supplies. Nevertheless, to make the system more realistic in the study, the grid voltage signal is sent out to the real world and then again sent back to test algorithms through an analog-to-digital converter (ADC) port of the DS1104 controller via the CLP-1104 board. Simultaneously, a four-channel (DL-9040) oscilloscope records a three-phase grid voltage signal and estimated parameters in real time. Nevertheless, due to the limitation of the ports in the DL-9040, the steps have to be reiterated for recording the estimated phase, frequency, and amplitude obtained from the proposed algorithm, respectively. The only difference is that once the grid voltage is recorded, then it is iteratively fed to the control algorithms to estimate a single parameter of interest and is sent out in real time via the DAC port of the CLP-1104 board to record variations in the estimated parameters on the DL-9040 in a sequential manner. The outcomes of test cases are framed in two ways: 1) numerical results for enhanced visualization and 2) experimental results for early validation, which are compared with both the PLL and PLL-less approaches (as discussed in Table 1). The evaluation report, focusing on grid disturbances, such as fundamental NS (FNS), DC-offset, harmonics, and variations in amplitude, phase, frequency, or their combinations, is numerically presented in Table 3.

A. TEST STUDY 1 (S-1)

Voltage Sag (0.4 pu), Δf =+2 Hz, and a Phase-Jump (+20°) With Harmonics: In the initial phase of the experiment, the grid was operating at the nominal frequency conditions. Under favorable grid circumstances, the voltage signal in the grid exhibited a significant and abrupt change at time $t = 1$ s. This change involved an increase in frequency by +2 Hz, a

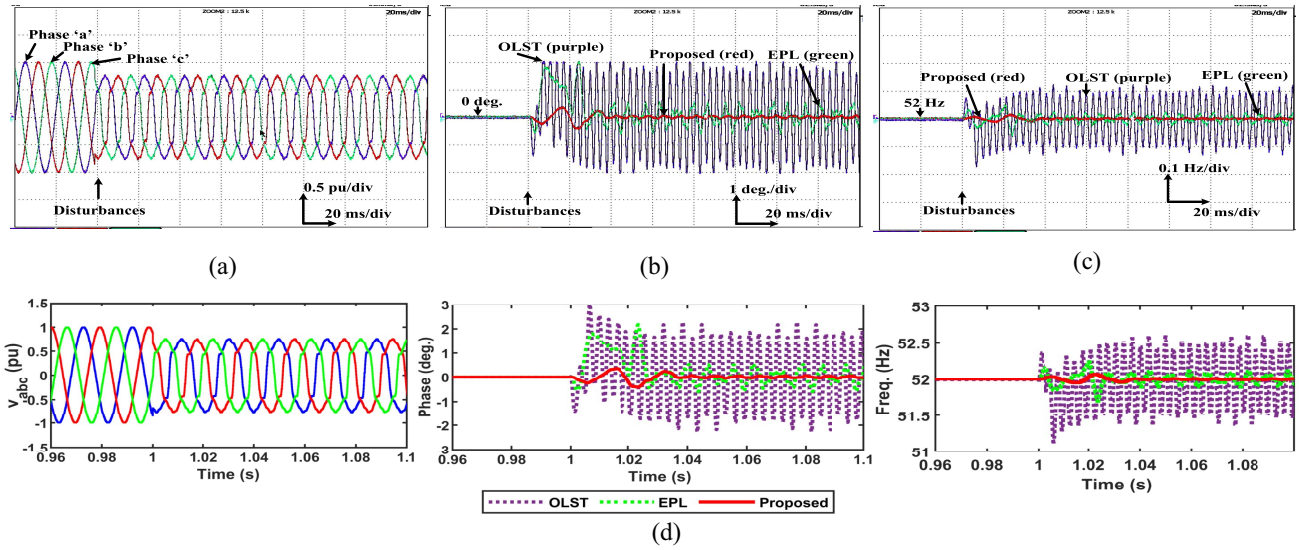

FIGURE 15. Test study S-4: experimental [15(a)–(c)] and simulation results [15(d)] in the presence of inter harmonics including voltage sag (0.2 pu). (a) Three-phase grid voltage. (b) Estimated actual phase-angle ($\hat{\theta}_{act}$). (c) Estimated fundamental frequency ($\hat{f}_g$). (d) Simulation results of S-4.

TABLE 2. Harmonics percentage of fundamental component as per the standard EN50160 [44].

Harmonics											
2^{nd}	3^{rd}	4^{th}	5^{th}	6^{th}	7^{th}	8^{th}	9^{th}	10^{th}	11^{th}	12^{th}	13^{th}
4%	10%	3%	8%	2%	5%	1%	3%	1%	2%	1%	1%

decrease in voltage by 0.4 per unit (pu), and a phase shift of 20°. The odd and even harmonic components involved in the grid voltage are outlined in Table 2. Fig. 12(j) presents a comparative analysis of the experimental and simulated results using different techniques. It is worth highlighting that the proposed method exhibited an exceptional ability to maintain a stable frequency estimation with a minimal transient variation of only 1 Hz, a performance that significantly surpassed other techniques. In contrast, the CDSC-PLL, OLST, and EPL methods displayed relatively larger transient variations of 2.78, 2.4, and 2.0 Hz, respectively. Furthermore, when it comes to steady-state accuracy, the proposed method consistently outperformed its counterparts, with CDSC-PLL, OLST, and EPL exhibiting oscillations of 0.06, 0.93, and 0.03 Hz, respectively. All methods demonstrated commendable ability in accurately tracking the voltage drop that occurred within the utility grid. Regarding the precision of the phase estimation process, the proposed synchronization approach, CDSC-PLL, OLST, and EPL exhibited transient deviations of approximately 3.0°, 13.1°, 4.81°, and 4.1°, respectively.

B. TEST STUDY 2 (S-2)

FNS (0.33 pu), Phase-Jump of (+20°) and Harmonics: This study evaluates how well the current proposal behaves under the challenging conditions, such as faults in the power system and phase jumps with even and odd-order harmonics (see Table 2). At the beginning of the test, the grid was operating at its nominal frequency of 50 Hz. Considering the simulation test scenario [see Fig. 13(e)], at $t = 1$s, the voltage in one phase of the grid became zero, and the experimental conditions are shown in Fig. 13(a)–(d). The proposed technique outperforms all other methods in terms of estimating the frequency. It achieves a new steady state within 27 ms and has a peak overshoot of 2.9 Hz, which is lower than the overshoot produced by CDSC-PLL, OLST, and EPL (3.4, 7.2, and 4.0 Hz, respectively). All approaches, including the proposed method, can estimate the FFPS amplitude. The most critical task is to accurately estimate the grid voltage phase angle. The highest transient phase deviation of 12.5° is offered by the OLST, which has 11.9° of oscillations in the steady state compared to other schemes. From this test study it can be concluded that the proposed technique can accurately estimate grid voltage parameters, even under challenging conditions, such as power system faults and phase jumps with harmonics.

C. TEST STUDY 3 (S-3)

Dc-Offset (10% in Phase 'a', −20% in Phase 'b', and +20% in Phase 'c') Under Frequency Drift of 5 Hz (47 Hz–52 Hz) With Harmonics: Dc-offset is often caused by various factors, such as transformer core saturation, ADCs, and single-phase rectifiers. This study takes into account the effects of frequency drift, phase jumps, and harmonics (odd order from Table 2), along with dc-offsets. The frequency was stepped from 47 to 52 Hz and the phase voltages (denoted as v_a, v_b, and v_c) were influenced by dc-offsets of 10%, -20%, and +20% of their previous amplitudes. These uneven dc-offset posed a challenge for accurately estimating grid voltage parameters, including frequency, phase, and amplitude. Despite these challenges, the proposed technique demonstrated superior accuracy in parameter estimation when compared to other methods. The results, as depicted

TABLE 3. Comparative analysis under various grid conditions.

Adverse Test Studies		Advanced grid synchronization techniques [23]	[42]	[41]	Proposed
S-1	Δf_t (Hz)	2.78	2.41	2.0	1
	Δf_s (Hz)	0.06	0.93	0.029	≈ 0
	$\Delta\theta_t$ ($^\circ$)	13.8	4.81	4.1	4
	$\Delta\theta_s$ ($^\circ$)	0.41	3.8	0.20	≈ 0
	t_s (ms)	≈ 35	≈ 20	≈ 25	27
S-2	Δf_t (Hz)	3.1	7.2	4.01	2.9
	Δf_s (Hz)	≈ 0	≈ 2.9	≈ 0	≈ 0
	$\Delta\theta_t$ ($^\circ$)	14.5	16.5	10.9	11.4
	$\Delta\theta_s$ ($^\circ$)	≈ 0	11.9	≈ 0	≈ 0
	t_s (ms)	≈ 35	≈ 20	≈ 25	27
S-3	Δf_t (Hz)	0.36	4.29	0.91	0.84
	Δf_s (Hz)	0.018	3.85	0.004	≈ 0
	ΔA_t (pu)	0.03	0.05	0.045	0.035
	ΔA_s (pu)	≈ 0.0004	≈ 0.02	≈ 0	≈ 0
	$\Delta\theta_t$ ($^\circ$)	20.2	17.4	16.8	18.5
	$\Delta\theta_s$ ($^\circ$)	0.11	13.5	0.04	≈ 0
	t_s (ms)	≈ 35	≈ 20	≈ 25	27

Inter-harmonic Test study		PLL-Less Methods [41]	[42]	Proposed
S-4	Δf_t (Hz)	0.3	0.7	0.025
	Δf_s (Hz)	0.12	0.6	0.007
	$\Delta\theta_t$ ($^\circ$)	2.1	3	0.3
	$\Delta\theta_s$ ($^\circ$)	0.5	2.1	0.065

where t_s represents the time taken for the system to reach a steady-state. The transient deviations in the estimated values of the fundamental frequency, phase, and amplitude from their true values are denoted by Δf_t, $\Delta\theta_t$, and ΔA_t, respectively. On the other hand, the steady-state errors in the estimated fundamental frequency, phase, and amplitude are represented by Δf_s, $\Delta\theta_s$, and ΔA_s, respectively.

in Fig. 14 (with a magnified view), reveal that the proposed technique maintained a good dynamic response of 27 ms with a good balance of steady-state accuracy.

D. TEST STUDY 4 (S-4)

Inter Harmonics Including Voltage Sag (0.2 pu): This rigorous test study investigates the impact of harmonics (dominating odd-order: 3rd & 5th and dominating even-order 2nd & 4th, their level is mentioned in Table 2), interharmonics (0.03 pu and 175 Hz), and subharmonics (0.02 pu and 25 Hz) on grid voltage under off-nominal conditions, resulting in a voltage loss of 0.2 pu. Fig. 15 illustrates the performance of each comparative scheme. When the grid voltage is exposed to interharmonics and harmonics, it becomes evident that all schemes exhibit steady-state oscillations in both the frequencies (0.6, 0.12, and 0.007 Hz) and phase (2.1°, 0.5°, and 0.065°) in OLST, EPL, and the proposed scheme, respectively. Nonetheless, the proposed method displays fewer steady-state oscillations and demonstrates greater resilience in addressing these challenges compared to the conventional methods. Also, Table 3 offers numerical data for understanding the ability of the interharmonic suppression with the current proposal and demonstrates superior accuracy in the steady state under off-nominal frequency conditions. Hence, without a doubt, the effectiveness of the proposed scheme surpasses that of the other well-established grid synchronization methods.

VII. CONCLUSION

In order to overcome the drawbacks associated with the PLL, a PLL-less grid synchronization scheme is developed in this article. In this context, a newly designed CBPF shows high disturbance rejection capability and is capable enough for extraction of FFPS components from a harmonically polluted grid condition. Moreover, the proposed FEA accurately estimates the fundamental frequency of the grid voltage. Additionally, using the error compensation technique, amplitude, and phase angle can be adaptively estimated. The present article incorporated the detailed design procedure, mathematical calculation, and control parameters, which makes them relatively simpler to implement in a real-time environment. The proposed grid synchronization technique is evaluated under a variety of challenging grid conditions, such as FFNS, dc-offset, harmonics, and interharmonics. Nonetheless, comparative analyses of the experimental and simulation results demonstrate that the proposed approach outperforms all other comparable techniques. It exhibits higher resiliency, robustness, and accuracy, maintaining a fast dynamic speed while estimating the grid voltage parameters. The proposed technique could, therefore, be a suitable alternative for synchronizing three-phase grid converters.

REFERENCES

[1] "Climate change performance index." 2022. [Online]. Available: https://ccpi.org

[2] J. Tian, C. X. Mao, D. Wang, S. X. Nie, and Y. Yang, "A shorttime transition and cost saving redundancy scheme for medium-voltage three-phase cascaded H-bridge electronic power transformer," *IEEE Trans. Power. Electron.*, vol. 33, no. 11, pp. 9242–9252, Nov. 2018.

[3] B. Aurobinda, S. Bidyadhar, and K. R. Pravat, "A combined reinforcement learning and sliding mode control scheme for grid integration of a PV system," *CSEE J. Power Energy Sys.*, Vol. 5, no. 4, pp. 498–506, Dec. 2019.

[4] R. Teodorescu, M. Liserre, and P. Rodríguez, *Grid Converters for Photovoltaic and Wind Power Systems*, Hoboken, NJ, USA: Wiley-IEEE Press, 2011.

[5] F. Blaabjerg, R. Teodorescu, M. Liserre, and A. V. Timbus, "Overview of control and grid dc-offset for distributed power generation systems," *IEEE Trans. Ind. Electron.*, vol. 53, no. 5, pp. 1398–1409, Oct. 2006.

[6] M. A. Perez, J. R. Espinoza, L. A. Moran, M. A. Torres, and E. A. Araya, "A robust phase-locked loop algorithm to synchronize static-power converters with polluted AC systems," *IEEE Trans. Ind. Electron.*, vol. 55, no. 5, pp. 2185–2192, May 2008.

[7] T. Xia. X. Zhang, G. Tan, and Y. Liu, "Synchronous reference frame single-phase phase-locked loop (PLL) algorithm based on half-cycle DFT," *Inst. Eng. Technol. Power Electron.*, vol. 13, no. 9, pp. 1893–1900, Jul. 2020.

[8] S. Golestan, M. Monfared, and F. D. Freijedo, "Design-oriented study of advanced synchronous reference frame phase-locked loops," *IEEE Trans. Power. Electron.*, vol. 28, no. 2, pp. 765–778, Feb. 2013.

[9] F. Liccardo, P. Marino, and G. Raimondo, "Robust and fast three-phase PLL tracking system," *IEEE Trans. Ind. Electron.*, vol. 58, no. 1, pp. 221–231, Jan. 2011.

[10] S. Golestan, M. Ramezani, J. M. Guerrero, F. D. Freijedo, and M. Monfared, "Moving average filter based phase-locked loops: Performance analysis and design guidelines," *IEEE Trans. Power Electron.*, vol. 29, no. 6, pp. 2750–2763, Jun. 2014.

[11] A. Elrayyah, Y. Sozer, and M. Elbuluk, "Robust phase locked-loop algorithm for single-phase utility-interactive inverters," *Inst. Eng. Technol. Power Electron.*, vol. 7, no. 5, pp. 1064–1072, May 2014.

[12] I. Carugati, S. Maestri, P. G. Donato, D. Carrica, and M. Benedetti, "Variable sampling period filter PLL for distorted three-phase systems," *IEEE Trans. Power Electron.*, vol. 27, no. 1, pp. 321–330, Jan. 2012.

[13] S. Golestan, J. M. Guerrero, A. Vidal, A. G. Yepes, and J. Doval-Gandoy, "PLL with MAF-based prefiltering stage: Small-signal modeling and performance enhancement," *IEEE Trans. Power. Electron.*, vol. 31, no. 6, pp. 4013–4019, Jun. 2016.
[14] F. Gonzalez-Espin, E. Figueres, and G. Garcera, "An adaptive synchronous-reference-frame phase-locked loop for power quality improvement in a polluted utility grid," *IEEE Trans. Ind. Electron.*, vol. 59, no. 6, pp. 2718–2731, Jun. 2012.
[15] M. A. Akhtar and S. Sahaa, "Analysis and comparative studies on impact of transport delay and transforms on the performance of TD-PLL for single phase GCI under grid disturbances," *Int. J. Elec. Power Energy System.*, vol. 115, no. 6, Feb. 2020, Art. no. 105488.
[16] S. Golestan, J. M. Guerrero, and J. C. Vasquez, "Three-phase PLLs: A review of recent advances," *IEEE Trans. Power. Electron.*, vol. 32, no. 3, pp. 1894–1907, Mar. 2017.
[17] F. Xiao, L. Dong, L. Li, and X. Liao, "A frequency-fixed SOGI-based PLL for single-phase grid-connected converters," *IEEE Trans. Power. Electron.*, vol. 32, no. 3, pp. 1713–1719, Mar. 2017.
[18] A. Luna et al., "Grid voltage synchronization for distributed generation systems under grid fault conditions," *IEEE Trans. Ind. Appl.*, vol. 51, no. 4, pp. 3414–3425, Jul./Aug. 2015.
[19] A. Luo, Y. Chen, Z. Shuai, and C. Tu, "An improved reactive current detection and power control method for single-phase photovoltaic grid-connected DG system," *IEEE Trans. Energy Conv.*, vol. 28, no. 4, pp. 823–831, Dec. 2013.
[20] W. Li, X. Ruan, C. Bao, D. Pan, and X. Wang, "Grid synchronization systems of three-phase grid-connected power converters: A complex-vector-filter perspective," *IEEE Trans. Ind. Electron.*, vol. 61, no. 4, pp. 1855–1870, Apr. 2014.
[21] X. Guo, W. Wu, and Z. Chen, "Multiple-complex coefficient-filter-based phase-locked loop and dc-offset technique for three-Phase grid-interfaced converters in distributed utility networks," *IEEE Trans. Ind. Electron.*, vol. 58, no. 4, pp. 1194–1204, Apr. 2011.
[22] M. Chen, L. Peng, B. Wang, and W. Wu, "Accurate and fast harmonic detection based on the generalized trigonometric function delayed signal cancellation," *IEEE Access*, vol. 7, pp. 3438–3447, 2019.
[23] F. Sevilmis and H. Karaca, "Implementation of enhanced non-adaptive cascaded DSC-PLLs for renewable energy systems," *Int. J. Elec. Power Energy System.*, vol. 134, Aug. 2021, Art. no. 1074470.
[24] S. Gude, C. C. Chu, and S. V. Vedula, "Recursive implementation of multiple delayed signal cancellation operators and their applications in prefiltered and in-loop filtered PLLs under adverse grid conditions," *IEEE Trans. Ind. Appl.*, vol. 55, no. 5, pp. 5383–5394, Oct. 2019.
[25] M. S. Reza and M. M. Hossain, "Recursive DFT-based method for fast and accurate estimation of three-phase grid frequency," *IEEE Trans. Ind. Electron.*, vol. 37, no. 1, pp. 49–54, Jan. 2022.
[26] J. Li, Q. Wang, L. Xiao, Y. Hu, Q. Wu, and Z. Liu, "An $\alpha\beta$-frame moving average filter to improve the dynamic performance of phase-locked loop," *IEEE Access*, vol. 8, pp. 180661–180671, 2020.
[27] M. S. Reza, M. M. Hossain, A. O. Nasif, and V. G. Agelidis, "Fast estimation of phase angle for three-phase voltage systems under distorted conditions," *IEEE J. Emer. Sel. Topics Power Electron.*, vol. 10, no. 3, pp. 2819–2828, Jun. 2022.
[28] M. Mellouli, M. Hamouda, J. B. H. Slama, and K. Al-Haddad, "A third-order MAF based QT1-PLL that is robust against harmonically distorted grid voltage with frequency deviation," *IEEE Trans. Energ. Conv.*, vol. 36, no. 3, pp. 1600–1613, Sep. 2021.
[29] O. Vainio, S. J. Ovaska, and M. Polla, "Adaptive filtering using multiplicative general parameters for zero-crossing detection," *IEEE Trans. Ind. Electron*, vol. 50, no. 6, pp. 1340–1342, Dec. 2003.
[30] M. Kumar, S. Pandit, and S. Chandrasekaran, "Cascaded sliding DFT based grid synchronization technique with DC offset removal capability," in *Proc. IEEE 21st Natl. Power Syst. Conf. (NPSC)*, 2020, pp. 1–6.
[31] E. Lavopa, P. Zanchetta, M. Sumner, and F. Cupertino, "Real-time estimation of fundamental frequency and harmonics for active shunt power filters in aircraft electrical systems," *IEEE Trans. Ind. Electron.*, vol. 56, no. 8, pp. 2875–2884, Aug. 2009.
[32] I. Kamwa, S. R. Samantaray, and G. Joos, "Wide frequency range adaptive phasor and frequency PMU algorithms," *IEEE Trans. Smart Grid*, vol. 5, no. 2, pp. 569–579, Mar. 2014.
[33] M. S. Reza, M. Ciobotaru, and V. G. Agelidis, "Robust estimation of real-time single-phase grid voltage frequency under distorted conditions," in *Proc. IEEE ECCE Asia Downunder*, 2013, pp. 948–954.
[34] H. A. Darwish and M. Fikri, "Practical considerations for recursive DFT implementation in numerical relays," *IEEE Trans. Power Del.*, vol. 22, no. 1, pp. 42–49, Jan. 2007.
[35] G. Fedele, C. Picardi, and D. Sgro, "A power electrical signal tracking strategy based on the modulating functions method," *IEEE Trans. Ind. Electron.*, vol. 56, no. 10, pp. 4079–4087, Oct. 2009.
[36] M. S. Reza, M. M. Hossain, and M. Ciobotaru, "Teager energy operator for fast estimation of three-phase grid frequency," *IEEE Trans. Instrum. Meas.*, vol. 70, pp. 1–10, 2021. [Online]. Available: https://ieeexplore.ieee.org/document/9210084
[37] A. Lopez, J. Montano, M. Castilla, J. Gutierrez, M. D. Borras, and J. C. Bravo, "Power system frequency measurement under non-stationary situations," *IEEE Trans. Power Del.*, vol. 23, no. 2, pp. 562–567, Apr. 2008.
[38] P. R. Sanchez, X. del Toro Garcia, A. P. Torres, and V. Feliu, "Fundamental positive-and negative-sequence estimator for grid DC-offset under highly disturbed operating conditions," *IEEE Trans. Power Electron.*, vol. 28, no. 8, pp. 3733–3746, Aug. 2013.
[39] S. Golestan, J. M. Guerrero, and J. C. Vasquez, "An open-loop grid synchronization approach for single-phase applications," *IEEE Trans. Power Electron.*, vol. 33, no. 7, pp. 5548–5555, Jul. 2018.
[40] H. Ahmed, R. Ushirobira, and D. Efimov, "A simple frequency estimator for power systems," *IEEE Trans. Instrum. Meas.*, vol. 70, pp. 1–2, Jul. 2021. [Online]. Available: https://ieeexplore.ieee.org/document/9475553
[41] M. Kumar et al., "Enhanced PLL-less grid synchronization algorithm amidst unbalanced and distorted three-phase grid conditions," *Int. J. Electr. Power Energy Syst.*, vol. 148, Jan. 2023, Art. no. 108926.
[42] P. Liu and S. Duan, "An open-loop synchronization technique with simple structure for phase error compensation and frequency estimation," *IEEE Trans. Ind. Electron.*, vol. 67, no. 10, pp. 8936–8940, Oct. 2020.
[43] S. Golestan, M. Monfared, F. D. Freijedo, and J. M. Guerrero, "Design and tuning of a modified power-based PLL for single-phase gridconnected power conditioning systems," *IEEE Trans. Power Electron*, vol. 27, no. 8, pp. 3639–3650, Aug. 2012.
[44] *Voltage Characteristics of Electricity Supplied by the Public Distribution System*, European Standard EN 50160, 2008.
[45] *Testing and Measurement Techniques—General Guide on Harmonics and Interharmonics Measurements and Instrumentation, for Power Supply Systems and Equipment Connected Thereto*, IEC Standard 61000-4-7, 2002.
[46] R. G. Lyons, *Understanding Digital Signal Processing*, 3rd ed. London, U.K.: Pearson, 2011, pp. 53–126.

MANISH KUMAR received the B.Tech. degree in electrical engineering from Rajiv Gandhi Proudyogiki Vishwavidyalaya, Bhopal, India, in 2014, the M.Tech. degree in control system engineering from the National Institute of Technology (NIT), Patna, India, in 2017, and the Ph.D. degree in electrical engineering, NIT, Hamirpur, India, in 2023.

He is an Active Researcher with the Field of Power Electronics and Control. His research work includes grid synchronization, drive and control, power quality improvement, and electric vehicle.

ANANT KUMAR VERMA (Member, IEEE) received the bachelor's degree in instrumentation engineering from the University Science Instrumentation Center, Srinagar, India, in 2012, the master's degree in power electronics and drives from Dehradun Institute of Technology, Dehradun, India, in 2014, and the Ph.D. degree in electrical engineering from the National Institute of Technology, Hamirpur, India.

He is currently a Postdoctoral Fellow with the Universidad de O'Higgins, Rancagua, Chile.

CLAUDIO BURGOS-MELLADO (Senior Member, IEEE) received the B.Sc. and M.Sc. degrees in electrical engineering from the University of Chile, Santiago, Chile, in 2012 and 2013, respectively, and the dual Ph.D. degree in electrical and electronic engineering from the University of Nottingham, Nottingham, U.K., and the University of Chile in 2019.

He is currently an Assistant Professor with the Institute of Engineering Sciences, Universidad de O'Higgins, Rancagua, Chile.

RAJ KUMAR JARIAL (Member, IEEE) received the B.Sc.Engg. degree in electrical engineering and the master's degree in power system from the National Institute of Technology (NIT), Kurukshetra, India, in 1989 and 1992, respectively.

Since 1994, he has been with the Department of Electrical Engineering, where he is currently serving as an Associate Professor with NIT, Hamirpur, India. His current research interest includes power electronics based drives and high voltage engineering.

RAVINDER NATH received the B.E. degree in electrical engineering from Madan Mohan Malviya Engineering College, Gorakhpur, India, in 1987, the M.Tech. degree in electrical engineering (control system) from the National Institute of Technology (NIT), Kurukshetra, India, in 1991, and the Ph.D. degree in electrical engineering from the Indian Institute of Technology at Kanpur, Kanpur, India, in 2006.

He joined with NIT, Kurukshetra, as a Lecturer in the year 1989 and then NIT, Hamirpur, in 1990, where he is currently working as an Associate Professor with the Department of Electrical Engineering. His research interests include signal processing, communication systems, and control systems.

BHUMAIAH JULA received the B.Tech. degree in electrical and electronics engineering and the M.Tech. degree in power electronics and electrical drives from Jawaharlal Nehru Technological University, Hyderabad, India, in 2009 and 2013, respectively. He is currently pursuing the Ph.D. degree in the field of converter control connected to electric aircraft grid and utility grid with the National Institute of Technology, Hamirpur, India.

DIEGO MUÑOZ-CARPINTERO (Member, IEEE) received the B.Sc. and M.Sc. degrees in electrical engineering from the Universidad de Chile, Santiago, Chile, in 2009 and 2010, respectively, and the D.Phil. degree in control engineering from the University of Oxford, Oxford, U.K., in 2014.

He is currently an Assistant Professor with the Institute of Engineering Science, Universidad de O'Higgins, Rancagua, Chile. His research interests include the areas of microgrids and electric vehicle routing.

CATALINA GONZÁLEZ-CASTAÑO received the degree in electronic engineering from the Universidad Nacional de Colombia, Manizales, Colombia, in 2008, the M.Eng. degree in electrical engineering from the Universidad Tecnológica de Pereira, Pereira, Colombia, in 2013, and the Ph.D. degree (Hons.) in electronic engineering in the field of power converters for electric vehicles from the Universitat Rovira i Virgili, Tarragona, Spain, in 2019.

She undertook her doctoral internship with the Advanced Center of Electrical and Electronic Engineering, Valparaiso, Chile. Her main research interests include electric power quality, vehicular power systems, and design and digital control of power converters.

PEDRO RONCERO-SÁNCHEZ (Senior Member, IEEE) received the M.Sc. degree in electrical engineering from the Universidad Pontificia Comillas, Madrid, Spain, in 1998, and the Ph.D. degree from the University of Castilla-La Mancha, Ciudad Real, Spain, in 2004.

He is currently an Associate Professor with the School of Industrial Engineering, University of Castilla-La Mancha. His research interests include control of power electronic converters, power quality, renewable energy systems, energy storage devices, and wireless power transfer.